Marine Structures 60 (2018) 201–217

Contents lists available at ScienceDirect

Marine Structures

journal homepage: www.elsevier.com/locate/marstruc

A global slamming force model for offshore wind jacket structures

Ying Tu[a], Zhengshun Cheng[b,*], Michael Muskulus[a]

[a] Department of Civil and Environmental Engineering, Norwegian University of Science and Technology, Høgskoleringen 7A, 7491 Trondheim, Norway
[b] Department of Marine Technology, Centre for Autonomous Marine Operations and Systems, Norwegian University of Science and Technology, Otto Nielsens veg 10, 7491 Trondheim, Norway

ARTICLE INFO

Keywords:
Wave slamming force
Jacket structure
Experiment
Global force
Plunging breaking wave

ABSTRACT

Under certain harsh environmental conditions, jacket structures supporting offshore wind turbines might be exposed to plunging breaking waves, causing slamming forces that affect the structural integrity and fatigue life. The slamming forces should thus be properly considered during the design, but a suitable force model specifically for jacket structures is currently in absence. In this study, a five-parameter force model is developed for estimating global slamming forces due to plunging breaking waves on jacket structures, based on statistical analyses of experimental data from the WaveSlam project. The force model is developed by considering a total of 176 individual breaking waves, under six wave conditions. For each individual breaking wave, the time history of the slamming force is calculated based on hammer test data in addition to wave test data, and the wave parameters are acquired from a wave elevation measurement. The acquired time histories and wave parameters are then used to determine the parameters involved in the force model, including two exponential parameters (i.e. α_1 and α_2) and three dimensionless coefficients for the expressions of wave-dependent parameters (i.e. duration coefficient ζ_1, rising time coefficient ζ_2, and peak force coefficient ζ_3). It is found that α_1, α_2, ζ_1 and ζ_2 are approximately constant, and ζ_3 follows a lognormal distribution. The quantile that determines ζ_3 should be carefully selected so as to provide a conservative prediction. A quantile of 95% is suggested in this paper, and it is found to be conservative based on the verification of the developed force model. Therefore, for a given sea state, this force model can give a deterministic and conservative prediction of the slamming force time history, regardless of the randomness of slamming forces. Challenges for the application of the force model are also addressed.

1. Introduction

Currently, the development of offshore wind energy is mainly in shallow or intermediate water, where bottom-fixed substructures (e.g. monopiles and jacket structures) are mainly used. Under harsh environmental conditions at certain locations, these substructures are exposed to plunging breaking waves, which cause slamming forces. The slamming force features an extremely high impact force within a very short time. It can affect the integrity and fatigue life of the substructures of offshore wind turbines (OWTs). Therefore, slamming forces should be properly considered in the design of OWTs that are likely to be exposed to plunging breaking waves.

Slamming, violent impact on offshore structures, is a strongly nonlinear phenomenon involving the interaction among water, air and structure. Slamming forces are affected by various factors, such as compressibility of water, hydroelasticity of the structure, air bubbles entrapped, cavitation and ventilation etc. [1]. In the past decades, a large amount of effort has been made to investigate this

* Corresponding author.
E-mail address: zhengshun.cheng@ntnu.no (Z. Cheng).

https://doi.org/10.1016/j.marstruc.2018.03.009
Received 4 December 2017; Received in revised form 26 February 2018; Accepted 19 March 2018

Table 1
Comparison of different slamming force models for cylindrical structures (modified from Ref. [7]).

Author	Theory	Maximum C_s	Slam duration, t_s	Time history of slamming coefficient, $C_s(t)$
Goda et al. [8]	von Karman	π	$\frac{D}{2C_b}$	$\pi\left(1-\frac{2C_b}{D}t\right)$
Campbell and Weynberg [9]	Experimental study	5.15	$\frac{D}{C_b}$	$5.15\left(\frac{D}{D+19C_bt}+\frac{0.107C_bt}{D}\right)$
Cointe and Armand [10]	Wagner and matched asymptotic expansions	2π	$\frac{3D}{2C_b}$	$2\pi-\left(4.72-\ln\left(\frac{2C_b}{D}t\right)\right)\sqrt{\frac{2C_b}{D}t}$
Wienke and Oumeraci [4]	Wagner	2π	$\frac{13D}{64C_b}$	$2\pi-2\sqrt{\frac{2C_b}{D}t}\left(\tanh^{-1}\sqrt{1-\frac{C_b}{2D}t}\right)$ (for $0\le t\le\frac{D}{16C_b}$) $\pi\sqrt{\frac{1}{12}\frac{D}{C_bt'}}-\sqrt[4]{\frac{16}{3}\frac{C_b}{D}t'}\tanh^{-1}\sqrt{1-\frac{2C_b}{D}t'\sqrt{\frac{12C_b}{D}t'}}$ $t'=t-\frac{D}{64C_b}$ (for $\frac{D}{16C_b}\le t\le\frac{13D}{64C_b}$)
WiFi formulation [6]	Wagner	2π	$\frac{13D}{64C_b}$	a symmetric load shape

Note that C_s is the slamming coefficient, D is the diameter of the cylinder, C_b is breaking wave celerity. In the WiFi formulation, the slamming force is assumed to be symmetric in time around the crest when the crest touches the structure surface.

complex phenomenon. The first work to study slamming forces theoretically was done by von Karman [2] on the estimation of forces on the floats of landing seaplanes. Later, Wagner [3] investigated the slamming forces on cylindrical structures, and in his study, the cylinder was approximated as a flat plate. The main difference between von Karman method and Wagner method is that the latter takes the local rise of free surface into account. This difference affects the duration and the magnitude of the calculated slamming force. Though the work by Wagner [3] was conducted 85 years ago, it is still widely used nowadays.

The von Karman method and Wagner method are usually used to determine the slamming coefficient of the slamming force for cylindrical structures, but the time history of the slamming force is also important when considering the effect of the slamming force. Several force models that can describe the time history of the slamming forces on cylindrical structures were thus developed, as given in Table 1. In these models, the slamming coefficients are time dependent. The Wienke and Oumeraci [4] model is recommended by the IEC 61400-3 standard [5] for designing OWT support structures. The WiFi formulation was newly developed in the WiFi JIP (Joint Industry Project Wave Impacts on Fixed turbines) in 2017 [6].

The models given in Table 1 were derived by using different approaches. The von Karman theory was implemented by Goda et al. [8], and Wagner theory was employed by Wienke and Oumeraci [4]. In addition to Wagner method, Cointe and Armand [10] also derived the asymptotic expressions for the inner domain and outer domain at the spray root during the impact and further solved the problem by matching the inner and outer asymptotic expressions. Campbell and Weynberg [9] determined the slamming coefficient by experimental study. The WiFi formulation was developed based on a combination of Wagner method and model tests at MARIN (Maritime Research Institute Netherlands) and at Deltares. It should be noted that these models were originally developed for a two dimensional (2D) slamming problem, hence the vertical distribution of slamming load was not taken into account. When applying these models to three dimensional (3D) problems, the vertical force distribution is usually assumed to be uniform or triangular.

The force models given in Table 1 were developed for cylindrical structures and can be used to estimate slamming forces on monopiles for OWTs. However, these force models might not be suitable for jacket structures, though they consist of several cylindrical legs and braces. One reason is that the water surface that approaches a leg or a brace is affected by other legs and braces, causing a more complicated slamming scenario than that for cylindrical structures.

The slamming forces acting on jacket structures are thus different from those on cylindrical structures. For jacket structures, wave slamming forces should be estimated both locally and globally. The local slamming forces are important for the design of e.g. individual legs, while the global slamming forces are essential for the design of e.g. foundation systems. Based on the experimental data from the WaveSlam project, Jose [11] discussed local versus global loads from breaking waves. Tu et al. [12] investigated the global slamming loads due to plunging breaking waves on jacket structures. A total of 3910 time series of slamming forces were reconstructed and statistically analyzed. The mean slamming coefficient was found to be about 1.30 at a curling factor of 0.4. In that study, two wave slamming load models were also proposed, i.e. a simplified force model and a refined force model, to represent the temporal development of global wave slamming loads on jacket structures. However, only one wave condition was considered in Ref. [12]. More wave conditions are thus required to further refine and verify the proposed force model.

In this study, six different wave conditions from the WaveSlam project are further analyzed to propose a more accurate global slamming force model for jacket structures for offshore wind applications. Under each wave condition, one or several wave test runs with a number of regular waves were carried out. Based on the experimental data, global slamming forces acting on a jacket structure model are inversely calculated by using the method developed by Tu et al. [13]. The parameters of the measured waves and the reconstructed slamming forces are then used to determine the parameters in the force model by statistical analysis. Verification and application of this developed force model are also addressed.

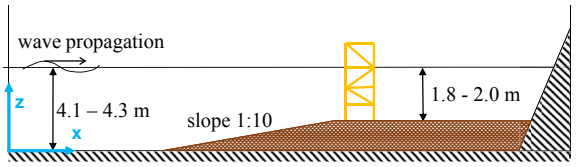

Fig. 1. Experimental setup and global coordinates [12]. The wave flume is about 300 m long, and the jacket is located at about 100 m before the end of the flume, with a much gentler slope than illustrated.

2. Experimental data

In this study, the experimental data from the WaveSlam project are used for the analyses. This project aims to improve the method for calculating slamming forces from plunging breaking waves on jacket structures through model tests on a large scale [14]. The project was conducted by a consortium headed by University of Stavanger (UiS) and Norwegian University of Science and Technology (NTNU) in 2012–2013. The experiment was conducted with a 1:8 scale model of a jacket structure, which is similar to the jacket designed by Reinertsen AS for the Thornton Bank offshore wind farm [15], using the Large Wave Flume facilities at the Coastal Research Centre (Forschungszentrum Küste, FZK)[1], Hannover, Germany. The experimental data have been released to the public since July 2015. The data used in this study are in model scale.

2.1. Experimental setup

The setup of the experiment is shown in Fig. 1. The wave flume is approximately 300 m long, 5 m wide and 7 m deep. The waves were generated by the wave board at the left end of the flume, went over a 1:10 slope, then reached the jacket model on a plateau. Since a water depth of 16 m was simulated, the water depth at the jacket model was set to 2.0 m for most cases. For some cases, the water depth was adjusted to 1.8 m. The diameter of the legs and the braces of the jacket model was 0.14 m.

A global coordinate system is defined as following: The origin is positioned at the middle position of the wave board ($x = 0$), at the bottom of the channel ($z = 0$) and at the south side of the flume, namely the right side when following the flow ($y = 0$). The x-axis is positive in the wave direction. The z-axis is positive upwards. The y-axis forms a right hand system with the other axes.

Wave gauges were installed at 15 different locations. Three Acoustic Doppler Velocity meters (ADVs) were installed in the plane of the legs. The motion of the wave paddle was also recorded. The jacket was equipped with four total force transducers, ten local force transducers on the legs, twelve XY force transducers on the braces, and four one-directional accelerometers.

The measurements taken by the total force transducers and by the wave gauge at the plane of the front legs of the structure are used in this study. Other measurements are not used, thus not described in detail as in the original data report [14]. As shown in Fig. 2, there were two total force transducers installed at the top of the jacket model and two installed at the bottom of the jacket model. The structure was hung from the top and did not touch the ground during the tests. The measured forces are in global x direction and have a sampling frequency of 10 kHz. The details of the transducers are illustrated in the figure as well. The names and locations of the transducers are introduced in Table 2. The location of the wave gauge is also shown in the table.

2.2. Selected wave test cases

For a proper statistical analysis, as many wave test runs under different wave conditions as possible should be included. Therefore, all the test runs in the WaveSlam project were checked, and the test runs to be analyzed were selected according to four criteria:

- The waves should be breaking.
- The breaking locations should be close to the plane of the front legs.
- The waves in the runs should be regular.
- The water depth of all the selected runs should match that of the used hammer test runs.

The selected test runs are illustrated in Table 3. They are all regular runs with breaking waves and have 2 m water depth at the structure. Ideally, only those runs in which the waves were breaking exactly at the plane of the front legs of the jacket structure should be used. However, the available runs under such condition are limited in number in the WaveSlam project and not enough for statistical analysis. Therefore, run 5 and run 6 are also included. Although the waves in these two runs broke 1 m in front of the structure, their breaking points were closest to the desired location among the rest of the available data.

The selected test runs under the same preset wave conditions are categorized into one case. Each case is described by a wave height and a wave period. The wave height and the wave period represent the values preset at the wave board for wave generation. They are not the ones measured at the structure or at the breaking point.

There are five other test runs in the WaveSlam data that seem to fulfill the criteria at a first glance. However, they are not used due to issues with the data quality, such as measurement errors and no obvious breaking at the front legs.

[1] https://www.fzk.uni-hannover.de/; November 2017.

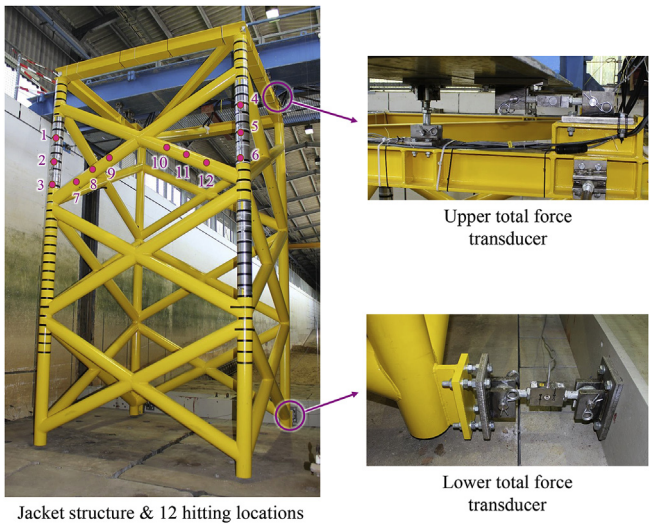

Fig. 2. Jacket structure, hammer hitting locations and total force transducers. Figures reprinted with permission from the WaveSlam project [12].

Table 2
The locations of total force transducers and wave gauge in global coordinates.

Transducer	Description	x [m]	y [m]	z [m]
FTTF01	Total force bottom south	200.961	1.405	2.465
FTTF02	Total force top south	200.265	1.405	6.935
FTTF03	Total force bottom north	200.961	3.655	2.465
FTTF04	Total force top north	200.265	3.655	6.935
WG S9	Wave elevation at front leg	198.37	0.60	7.00

Table 3
Selected wave test cases. The wave parameters as well as the rest of the data used in the study are in 1:8 model scale.

Case number	Wave height [m]	Wave period [s]	Location of breaking	Run number	Run ID in WaveSlam	Number of waves in test run	Used waves in test run
1	1.6	4.6	at front leg	1	20130614.04	20	2 to 20
2	1.65	4.6	at front leg	2	20130614.05	20	2 to 20
3	1.8	5.2	at front leg	3	20130618.03	10	2 to 6 and 8 to 10
				4	20130618.04	10	2 to 6 and 9 to 10
4	1.7	5.55	1 m in front of structure	5	20130614.24	20	2 to 20
5	1.7	5.2	1 m in front of structure	6	20130617.09	20	2 to 20
6	1.5	4.9	at front leg	7	20130617.15	20	3 to 19
				8	20130617.16	20	3 to 19
				9	20130617.17	20	3 to 19
				10	20130617.18	20	3 to 19
				11	20130617.19	20	3 to 19

Even from the selected runs, not all the waves are used for analysis. The very first waves in each run are not breaking, so they are discarded. Some waves in the runs lead to a small peak in front of the two main peaks in the response data, which implies earlier breaking compared to the other waves. These waves are also discarded. The used waves in each test run are listed in the last column of Table 3.

2.3. Hammer test cases for force reconstruction

The measured total forces during the wave tests are to be used for slamming force reconstruction to be discussed in Section 3.2. Apart from the wave test data, hammer test data are also essential for the reconstruction. The selected hammer test cases are the same as in Ref. [12] and listed in Table 4. The hammer tests were carried out in 2 m deep water, the same as for the selected wave cases. The structure was hit by a 1.5 kg impulse hammer in the wave direction. The impulse hammer recorded the time series of the forces exerted on the structure with a sampling frequency of 9600 Hz, in addition to the total force measurements. The hammer hit at twelve

Table 4
Selected hammer test cases [12].

Hit location number	Total hammer hits	ID of test run
1	6	24062013.14 ~ 16
2	4	24062013.17 ~ 18
3	4	24062013.22 ~ 23
4	6	24062013.31 ~ 33
5	8	24062013.34 ~ 37
6	6	24062013.38 ~ 40
7	2	24062013.24
8	2	24062013.25
9	2	24062013.26
10	2	24062013.27
11	2	24062013.28
12	2	24062013.30

locations in the front plane of the structure, both on the braces and on the legs. These locations (see Fig. 2) are in or close to the expected wave slamming zone for the wave tests. Since the hammer impacts were exerted manually, the locations shown in the figure are approximate. The number of hits for each location is different as shown in Table 4.

3. Calculation of slamming forces

The total force measurements of the wave test cases described in Section 2.2 cannot be analyzed directly, since they are just the response of the structure due to the wave forces. These measurements were used together with the hammer test data to calculate the slamming forces under the corresponding wave conditions. It is the calculated time series of the slamming forces that are used in later sections for the analyses and model development. The method for the calculation has been described in detail in Ref. [12], so it is summarized briefly below.

3.1. Pre-processing of the data

The total force measurements of the wave tests and hammer tests were processed by the following steps to get the *wave response forces* and *hammer response forces* used for slamming force reconstruction. A bandpass filter was first used to eliminate the high frequency noise (above 300 Hz) in the total force measurements. Then, the forces measured by the four transducers (see Fig. 2) were summed to obtain the total forces. Finally, a time domain robust LOESS smoother [16] was used to estimate the quasi-static part from the total force, and the dynamic part remains. It was confirmed in Ref. [17] that this smoother does not overestimate the peak of the quasi-static part, and is effective to resolve the dynamic part.

The impulse hammer measurements were resampled to 10 kHz to match the total force measurements, and the resampled *hammer impact forces* were used for slamming force reconstruction.

3.2. Reconstruction of wave slamming forces

The wave response force due to each wave was paired with the hammer test data of each hit at each location to reconstruct the slamming forces. The reconstructed forces are “effective forces”, which means that the wave slam is assumed to occur only on the corresponding hammer impact location. For each wave-hammer data pair, a force reconstruction method based on linear regression [13] was used. This reconstruction method has been verified in Ref. [13] by a method-to-method comparison.

The following briefly summarizes the force reconstruction method. The wave slamming force is expressed in vector form as

$$\mathbf{f_W} = \left(f_{W_1} \quad f_{W_2} \quad f_{W_3} \quad \cdots \quad f_{W_n}\right)^T \tag{1}$$

It can also be written as

$$\mathbf{f_W} = \mathbf{F_H}\,\boldsymbol{\beta} \tag{2}$$

where $\mathbf{F_H}$ is a matrix composed of column vectors representing repeated and shifted hammer impact forces and is given by

$$\mathbf{F_H} = \begin{pmatrix} f_{H_1} & 0 & \cdots & 0 \\ \vdots & \vdots & \ddots & \vdots \\ f_{H_\delta} & 0 & \ddots & 0 \\ f_{H_{\delta+1}} & f_{H_1} & \ddots & 0 \\ \vdots & \vdots & \ddots & \vdots \\ f_{H_{(p-1)\delta}} & f_{H_{(p-2)\delta}} & \ddots & 0 \\ f_{H_{(p-1)\delta+1}} & f_{H_{(p-2)\delta+1}} & \ddots & f_{H_1} \\ \vdots & \vdots & \ddots & \vdots \\ f_{H_n} & f_{H_{n-\delta}} & \cdots & f_{H_{n-(p-1)\delta}} \end{pmatrix} \tag{3}$$

in which the symbol p denotes the total number of hypothetical hammer hits. The symbol δ denotes the interval between every two hammer hits, and is named *step factor*. The step factor is set to 5 for most cases, according to [13].

The parameter vector $\boldsymbol{\beta}$ represents the coefficients for scaling the hammer hits and is given as

$$\boldsymbol{\beta} = (\beta_1 \;\; \beta_2 \;\; \beta_3 \;\; \cdots \;\; \beta_p)^T \tag{4}$$

Similarly, the wave response force is written in vector form as

$$\mathbf{r_W} = \left(r_{W_1} \;\; r_{W_2} \;\; r_{W_3} \;\; \cdots \;\; r_{W_n}\right)^T \tag{5}$$

It can also be expressed as

$$\mathbf{r_W} = \mathbf{R_H}\,\boldsymbol{\beta} + \mathbf{e} \tag{6}$$

where

$$\mathbf{R_H} = \begin{pmatrix} r_{H_1} & 0 & \cdots & 0 \\ \vdots & \vdots & \ddots & \vdots \\ r_{H_\delta} & 0 & \ddots & 0 \\ r_{H_{\delta+1}} & r_{H_1} & \ddots & 0 \\ \vdots & \vdots & \ddots & \vdots \\ r_{H_{(p-1)\delta}} & r_{H_{(p-2)\delta}} & \ddots & 0 \\ r_{H_{(p-1)\delta+1}} & r_{H_{(p-2)\delta+1}} & \ddots & r_{H_1} \\ \vdots & \vdots & \ddots & \vdots \\ r_{H_n} & r_{H_{n-\delta}} & \cdots & r_{H_{n-(p-1)\delta}} \end{pmatrix} \tag{7}$$

is composed of column vectors representing repeated and shifted hammer response forces, and

$$\mathbf{e} = (e_1 \;\; e_2 \;\; e_3 \;\; \cdots \;\; e_n)^T \tag{8}$$

is an error term due to the noise in the measurements.

The parameter vector $\boldsymbol{\beta}$ can be solved by applying an ordinary least squares regression technique based on Eq. (6), when $\mathbf{r_W}$ and $\mathbf{R_H}$ are known. The estimated parameter vector is given by

$$\hat{\boldsymbol{\beta}} = (\mathbf{R_H^T R_H})^{-1}\,\mathbf{R_H^T}\,\mathbf{r_W} \tag{9}$$

Knowing the hammer impact force and applying $\hat{\boldsymbol{\beta}}$ to Eq. (2), the wave slamming force is estimated as

$$\hat{\mathbf{f_W}} = \mathbf{F_H}\,\hat{\boldsymbol{\beta}} \tag{10}$$

3.3. Post-processing of the wave slamming forces

A reconstructed time series of slamming force contains two major peaks, corresponding to the wave impacts at the plane of the front legs and at the plane of the hind legs, respectively. Since the impact with larger force and impulse is of more importance in the design, only the first peak of the time series is considered in this study.

Four parameters were determined from each time series to describe the slamming forces, as illustrated in Fig. 3.

Since the wave response force due to each wave was paired with the hammer test data of each hit at each location to reconstruct the slamming forces, there are multiple force time series reconstructed for each wave impact. The slamming force due to each wave was obtained by averaging the reconstructed slamming forces. The averaging was performed in two steps and for both the time series and the parameters that describe the slamming force. When the time series were averaged, the peaks of them were aligned. We use symbol X to represent the time series or one of the parameters to be averaged. The subscripts h and l represent the indices of hit and location, respectively.

First, the values of different hits were averaged for each location of each wave.

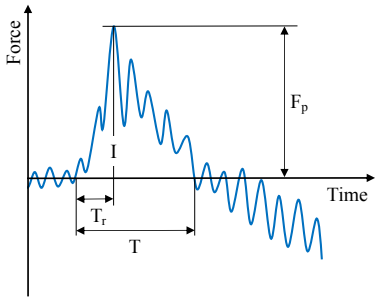

Fig. 3. Parameters to describe the force time series of one wave slamming event. The variation of the time series has been exaggerated for visualization purposes.

- F_p: Peak force, the maximum force in the time series.
- T: Duration, the time between the last zero-up-crossing before the peak and the first zero-down-crossing after the peak.
- T_r: Rising time, the time between the last zero-up-crossing before the peak and the peak itself.
- I: Impulse, the integral of the force over the duration.

$$\overline{X_l} = \frac{1}{N_h(l)} \sum_{h=1}^{N_h(l)} X_{l,h} \tag{11}$$

The number of hits $N_h(l)$ depends on the location (see Table 4).
Second, the averaged values of different locations were again averaged for each wave.

$$\overline{X} = \frac{1}{12} \sum_{l=1}^{12} \overline{X_l} \tag{12}$$

The purpose of the averaging is to obtain a single force time series that represents the wave hitting the front plane of the structure. Impacts at different locations result in slightly different responses (impulse response functions). The 12 locations for which hammer tests were performed sample the variability due to the impact location (studied in more detail in Ref. [12]). The average of the response from these 12 cases is considered the best available estimate of the response due to a wave hitting the front of the jacket at potentially different locations. In other words, what is averaged out is not noise or inherent randomness of the waves, but rather uncertainty regarding the exact positions on the structure where the wave hits (and in which sequence).

The resulting time series and parameters for all the waves described in Table 3 are used for the analyses in the next sections.

4. Model development

In Ref. [12], two parameterized models were proposed to describe the time series of the global slamming forces on jacket structures: a three-parameter simplified model and a five-parameter refined model. The refined model turned out to represent the force time series more accurately than the simplified one. Therefore, in this section, the refined model is further elaborated based on the slamming forces acquired by using the multiple wave cases in Table 3.

The original refined model is

$$f(t) = \begin{cases} F_p \exp\left(\alpha_1 \frac{t-t_p}{T_r}\right) & t_p - T_r < t \le t_p \\ F_p \exp\left(\alpha_2 \frac{t-t_p}{T-T_r}\right) & t_p < t \le t_p - T_r + T \\ 0 & \text{Otherwise} \end{cases} \tag{13}$$

where $f(t)$ is the time series of global slamming force; t_p denotes the moment of the peak in the time series; α_1 and α_2 are two parameters that determine the rate of exponential decay on both sides of the peak; peak force F_p, duration T and rising time T_r are three parameters determined by wave conditions.

Equation (13) can be transformed into

$$\ln\left(\frac{f(t)}{F_p}\right) = \begin{cases} \alpha_1 \frac{t-t_p}{T_r} & t_p - T_r < t \le t_p \\ \alpha_2 \frac{t-t_p}{T-T_r} & t_p < t \le t_p - T_r + T \\ 0 & \text{Otherwise} \end{cases} \tag{14}$$

The moment of peak t_p can be set to an arbitrary value. For simplification, it is set to zero, so Equation (14) becomes

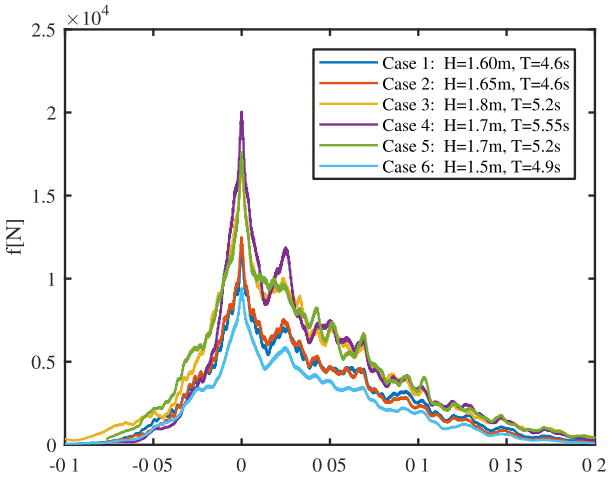

Fig. 4. Averaged force time series for six cases.

$$\ln\left(\frac{f(t)}{F_p}\right)=\begin{cases}\alpha_1\frac{t}{T_r} & -T_r<t\le 0\\ \alpha_2\frac{t}{T-T_r} & 0<t\le T-T_r\\ 0 & \text{Otherwise}\end{cases} \tag{15}$$

In order to apply the model in engineering practice, the five unknown parameters in the model have to be decided. They are discussed separately in two groups below, according to their features.

4.1. Determination of exponential parameters

The reconstructed time series of global slamming forces due to different waves in each case are averaged. The averaged force time series for the available six cases are plotted in Fig. 4. The peaks of the time series are aligned in the figure.

For all the six cases, the force seems to decay exponentially on both sides of the peak, which is in accordance with the proposed model.

The time series in Fig. 4 are then converted according to Equation (15) using the corresponding parameters F_p, T and T_r of each case. $\ln\left(\frac{f(t)}{F_p}\right)$ is plotted versus $\frac{t}{T_r}$ before the peak and versus $\frac{t}{T-T_r}$ after the peak in Fig. 5.

From the figure, $\ln\left(\frac{f(t)}{F_p}\right)$ is found to behave almost linearly with respect to $\frac{t}{T_r}$ before the peak and with respect to $\frac{t}{T-T_r}$ after the peak, which to some extent confirms the exponential behavior of the force time series.

To quantify this linear relationship between the horizontal axis value and the vertical axis value in Fig. 5, the mean $\mu(t)$ and

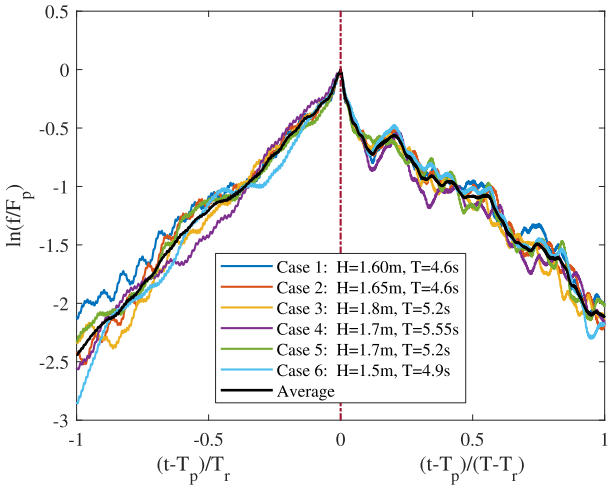

Fig. 5. Averaged force time series for six cases converted to Equation (15).

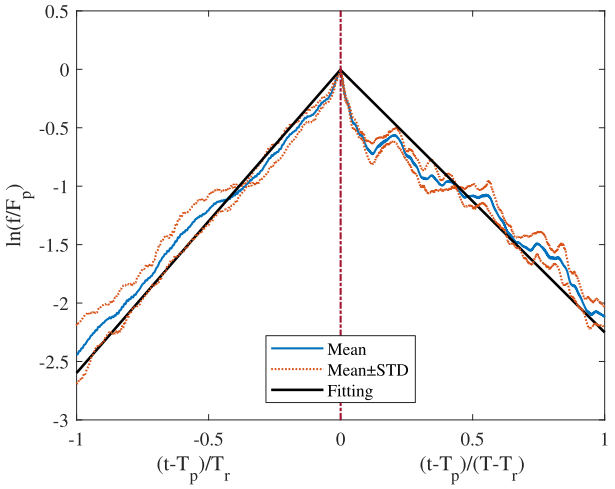

Fig. 6. Fitting of converted average force time series.

standard deviation $\sigma(t)$ of the six converted time series are estimated, as depicted in Fig. 6.

The standard deviation represents the variation of $\ln\left(\frac{f(t)}{F_p}\right)$ across the different wave conditions, and its value varies with the horizontal axis value. The variation of the slamming force time series due to the waves under the same preset condition ("Case" in this study) was discussed in detail in Ref. [12], and is thus not elaborated in the present study. However, the coefficient of variation (or relative standard deviation, $C_v(t) = \frac{\sigma(t)}{|\mu(t)|}$) varies only slightly with the horizontal axis value and has a low value of 0.08 on average. This implies that the variation among the time series are small, and it is plausible to use the mean curve to represent the six time series. It is found that the standard deviation in the vicinity of the peak is smaller than that far away from the peak. Since the force around the peak contributes the most to the impulse caused by a wave impact, it is important to estimate the force around the peak more accurately than the rest of the time series. Therefore, weighted linear regression [18] is applied to fit the mean time series on both sides of the peak. In weighted linear regression, the weighting coefficients are assumed to be inversely proportional to the variance (square of standard deviation), so a smaller standard deviation results in a larger weighting coefficient. This leads to higher weighting around the peak, where the standard deviation is lower. By using the fitting, the exponential parameters are determined: $\alpha_1 = 2.60$ and $\alpha_2 = -2.24$. The coefficients of determination, i.e. R^2 values, of the fitting are calculated using the same weighting scheme to be 0.9999 and 0.9992, respectively. This indicates that the exponential parameters α_1 and α_2 are determined with high confidence.

4.2. Determination of wave-dependent parameters

Given an arbitrary regular breaking wave condition, the other three parameters required by the model: duration T, rising time T_r and peak force F_p, are not known directly. However, they are wave-dependent parameters due to the physics, and can be determined by the given wave condition. In order to investigate the dependence of these parameters on the wave condition, three dimensionless coefficients are introduced.

The *duration coefficient* ζ_1 is defined as

$$\zeta_1 = \frac{T}{\frac{D_x}{C_b}} \tag{16}$$

where D_x is the equivalent width of the structure in the wave direction, the value of which depends on the structure geometry relative to the wave impact. Since the front legs and braces are all in a plane perpendicular to the wave direction and have the same diameter 0.14 m, this value is used for D_x. The breaking wave celerity C_b can be approximated by Equation (17), for shallow water waves with high steepness [19,20].

$$C_b = \sqrt{g(d + \eta_b)} \tag{17}$$

where g is the gravitational acceleration; d is the water depth; and η_b is the maximum elevation of the breaking wave, which can be obtained from the wave elevation measurement.

The *rising time coefficient* ζ_2 is defined as the ratio of rising time to duration.

$$\zeta_2 = \frac{T_r}{T} \tag{18}$$

The *peak force coefficient* ζ_3 is defined as

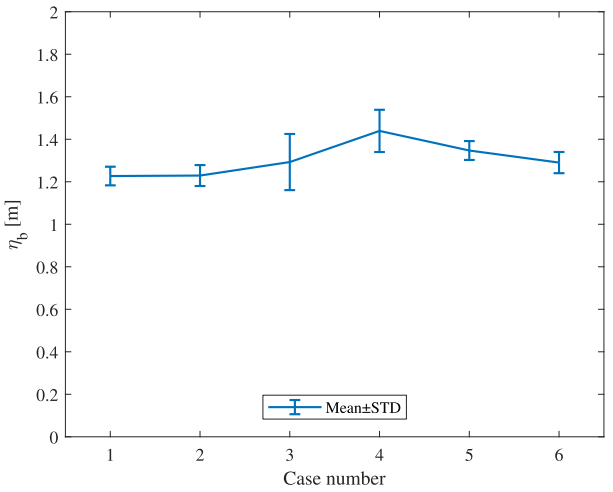

Fig. 7. Mean value and standard deviation of η_b in each case.

$$\zeta_3 = \frac{F_p}{\frac{1}{2}\rho D_y \eta_b C_b^2} = C_s \lambda \tag{19}$$

where ρ is the water density; D_y is the equivalent width of the structure in y-axis direction, the value of which depends on the structure geometry relative to the wave impact. For the investigated jacket, $D_y = 2 \times (1 + 2.15) \times 0.14$ m= 0.88m. Two inclined braces contribute 2.15 times their diameter 0.14m each to D_y, due to an inclined angle of 62° with respect to the vertical, while two vertical legs contribute one diameter each to D_y.

A typical formulation of three dimensional slamming force includes two coefficients: slamming coefficient C_s and curling factor λ. In some other studies, e.g. Wienke and Oumeraci [4], C_s was first determined theoretically, then λ was calculated empirically based on the determined C_s. In this study, C_s and λ are treated together as one coefficient ζ_3 instead, since they are not independent.

The values of ζ_1, ζ_2 and ζ_3 are calculated for each wave of the cases listed in Table 3. The η_b acquired from each single wave is the only essential wave parameter for the calculation. The mean and standard deviation of the input η_b values over each case are shown in Fig. 7. The variation of the calculated ζ_1, ζ_2 and ζ_3 are demonstrated in Figs. 8–10. In the figures, the result variation over different waves in each case is illustrated by the blue bars representing means and standard deviations. The result variation over different cases is illustrated by the red lines. The continuous red line represents the mean value calculated by averaging the means of each case. The dashed red lines represent the standard deviation of the means of each case.

From Figs. 8 and 9, it can be noticed that the variation of ζ_1 and ζ_2 over different cases is much smaller than the variation over different waves inside each case. The coefficients of variation of ζ_1 for the six cases range from 0.17 to 0.31, while the value over the six cases is only 0.06. Similarly, the coefficients of variation of ζ_2 for the six cases range from 0.20 to 0.34, while the value over the six cases is only 0.09. Although there is variability of ζ_1 and ζ_2 within each case, the means of all the cases are similar. This implies that ζ_1 and ζ_2 are insensitive to wave condition, so they are treated as constants because their mean values can be assumed to be the same for

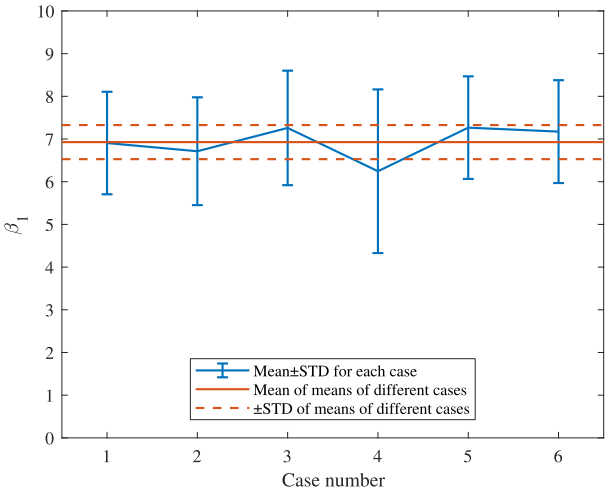

Fig. 8. Variation of ζ_1 in each case and over different cases.

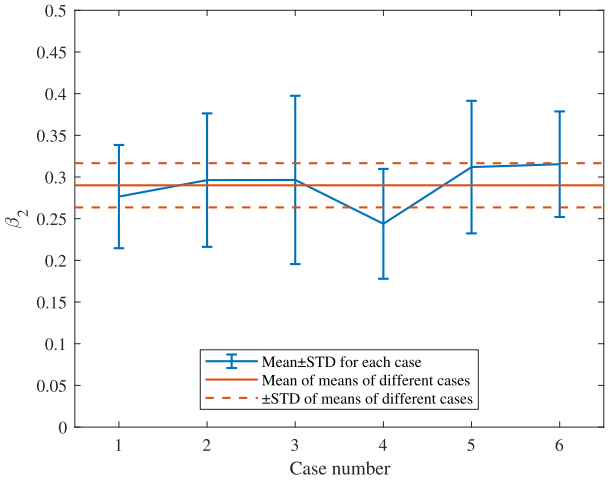

Fig. 9. Variation of ζ_2 in each case and over different cases.

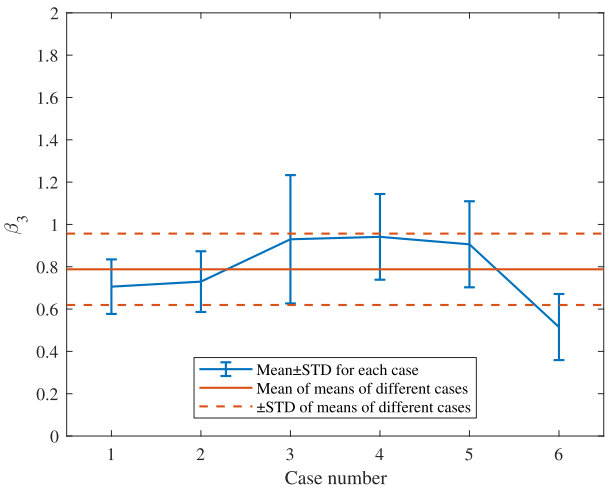

Fig. 10. Variation of ζ_3 in each case and over different cases.

different wave conditions.

The means and bootstrap 95% confidence intervals of ζ_1 and ζ_2 for each case are calculated and shown in Table 5. The confidence intervals are narrow compared to the mean values in general, so the means are representative for the cases. The duration coefficient and the rising time coefficient are therefore determined by averaging the means of each case, which leads to $\zeta_1 = 6.93$ with a 95% confidence interval of $\pm$ 0.32 and $\zeta_2 = 0.29$ with a 95% confidence interval of $\pm$ 0.02.

From Fig. 10, it can be noticed that the variation of ζ_3 over different cases is comparable to the variation over different waves inside each case. The coefficients of variation of ζ_3 for the six cases range from 0.18 to 0.33, and the coefficient over the six cases is 0.21. The coefficients of variation of the nominator and denominator in Eq. (19) over the six cases are 0.087 and 0.276, respectively.

Table 5
Means and bootstrap 95% confidence intervals of ζ_1 and ζ_2 for each case.

Case No.	ζ_1			ζ_2		
	Mean	Confidence interval		Mean	Confidence interval	
1	6.91	6.43	7.50	0.277	0.249	0.304
2	6.71	6.12	7.21	0.296	0.269	0.339
3	7.26	6.63	7.94	0.296	0.250	0.345
4	6.25	5.46	7.15	0.244	0.216	0.273
5	7.27	6.76	7.80	0.312	0.281	0.356
6	7.17	6.90	7.41	0.315	0.303	0.329

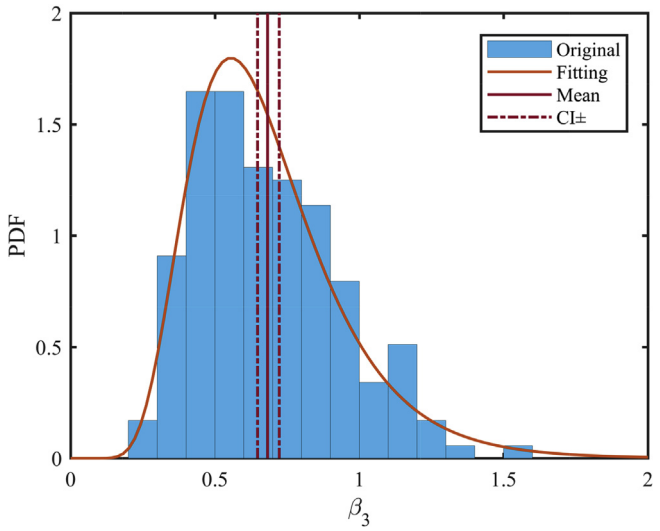

Fig. 11. Statistical properties of ζ_3, represented by histogram, distribution fitting by lognormal function, mean and confidence interval of the mean. The log location and log scale parameters of the lognormal distribution are -0.4497 and 0.3727, respectively.

So a constant value might not be representative enough for the peak force coefficient ζ_3. Attempts have been made to figure out the relationship between ζ_3 and the wave parameters, such as wave height, wave elevation and deep water wave length, and their ratios. However, the values of ζ_3 are much more widely spread than the values of those parameters and ratios, which does not support an expression of ζ_3 in terms of the wave parameters. The reason for such widely spread ζ_3 values could be explained by the slightly shifted breaking point relative to the jacket structure at each wave impact. Although the location of breaking is given for each test run in Table 3, it is based on the visual estimation for the whole run, and it is not strictly controlled for each wave in such a shallow water breaking wave test with many nonlinearities involved. Even if a wave breaks just slightly before or after the plane of the front legs, the peak force reduces significantly, thus changing the value of ζ_3 also significantly.

Since peak force is a decisive parameter for an accurate estimation of the slamming force time series and the total impulse exerted by a wave on the structure, the peak force coefficient ζ_3 should be determined with a more reliable approach. The ζ_3 values of all the waves in all the test runs are sorted in a histogram in Fig. 11. The data are then fitted by various distributions, and a lognormal distribution function is found to give the best goodness of fit among the commonly used distribution functions. The lognormal distribution function is thus selected, and its expression is given by

$$f(\zeta_3|\mu_L, \sigma_L) = \frac{1}{\sqrt{2\pi}\sigma_L\zeta_3}\exp\left\{\frac{-(\ln\zeta_3 - \mu_L)^2}{2\sigma_L^2}\right\} \tag{20}$$

in which μ_L and σ_L are the log location and log scale parameters, respectively. The fitted values for these two parameters are $\mu_L = -0.4497$ and $\sigma_L = 0.3727$. The log-likelihood of the fitting is 3.6.

The cumulative distribution function of ζ_3 based on the original data is plotted together with the fitted lognormal distribution in Fig. 12. From this figure, we can see more clearly that the lognormal distribution fits the data very well in general, although slight overestimation and underestimation exist locally. Four representative quantiles of the cumulative distribution function and their corresponding ζ_3 values are marked in Fig. 12, and the ζ_3 values from the fitted distribution are compared to those from the original data in Table 6. Since the cumulative distribution function based on the original data is discrete, the smallest available value that is larger than the given quantile is used for the calculation of ζ_3. In this way, ζ_3 can be well approximated when the number of data points at the quantile considered is very large; while for large quantile (e.g. 99%) where fewer data points are available, the approximated ζ_3 is likely to have a large uncertainty. Therefore, the relative difference between the two cumulative distribution functions is larger for the quantile of 99% than for the rest in the table. In this study, we use $\zeta_3 = 1.178$, which corresponds to the quantile of 95%, as a representative value for the peak force coefficient, because the quantile is relatively large, and the difference between the fitted distribution and the original data is relatively small for this quantile. In the application of the model, the peak force coefficient ζ_3 can be calculated from the lognormal distribution, according to the quantile needed for the design. Now that ζ_1, ζ_2 and ζ_3 have been determined, the wave-dependent parameters T, T_r and F_p of the force model can be calculated with Equations (16), (18) and (19), for a given structure and given wave conditions.

4.3. Application of the model

Knowing the five parameters determined in Sections 4.1 and 4.2, the model of the slamming force time series is completely defined. Once the site conditions and the structure properties are known, time series of the slamming force can be calculated. A flow chart as shown in Fig. 13 summarizes the procedure to get the force time series by applying the model. Knowing site conditions, the

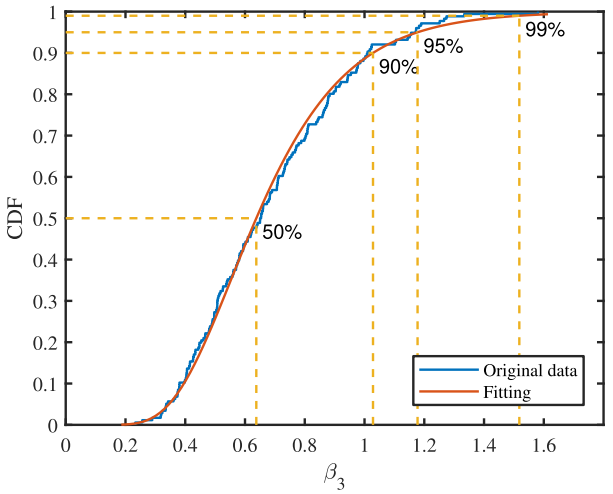

Fig. 12. Cumulative distribution function of ζ_3 based on the original data and the fitted lognormal distribution. Four representative quantiles and corresponding ζ_3 values are marked for the fitted distribution by the yellow lines. (For interpretation of the references to colour in this figure legend, the reader is referred to the Web version of this article.)

Table 6
Four representative quantiles and corresponding ζ_3 values estimated from the lognormal distribution and the original data.

Quantile [%]	ζ_3 from fitted CDF	ζ_3 from original CDF	Relative difference [%]
50	0.638	0.651	−2.00
90	1.028	1.009	1.88
95	1.178	1.172	0.51
99	1.518	1.334	13.79

wave parameters for the potential breaking waves are determined. Knowing both site conditions and structural properties, water depth d at the structure and the equivalent widths of the structure D_x and D_y are determined. The wave parameters and water depth are then used with suitable wave theories and breaking criteria to derive breaking wave celerity C_b and the maximum elevation of the breaking wave η_b. The determination of wave parameters and η_b for a given site condition is further addressed in Section 6. Then, the parameters D_x, D_y, C_b and η_b are used together with the coefficients ζ_1, ζ_2 and ζ_3 to calculate the wave-dependent parameters T, T_r and F_p. Finally, the wave-dependent parameters are used in the force model together with exponential parameters α_1, α_2 to obtain the time series of the slamming force $f(t)$.

5. Model verification

In this section, the developed model is verified against the original reconstructed time history of slamming force. Since the peak force F_p, duration T and rising time T_r are wave-dependent, the verification is thus conducted with respect to each individual wave. For the six wave conditions considered in this study, there are in total 176 individual waves. In each individual wave, both the wave parameters (such as wave height, wave period, maximum elevation η_b, etc.) and reconstructed time history of slamming force are available. Knowing water depth d and η_b, breaking wave celerity C_b is determined according to equation (17). Then by using parameters D_x, D_y, C_b and η_b together with coefficients ζ_1, ζ_2 and ζ_3, the wave-dependent parameters T, T_r and F_p are achieved. The time history of slamming force can then be predicted according to equation (15). Here four representative quantiles (i.e. 50%, 90%, 95%, 99%) are used when determining the ζ_3 value. An exemplary comparison between the original reconstructed slamming force and the predicted slamming forces by the force model is shown in Fig. 14.

In the verification, both peak force and impulse are considered. The predicted value is compared to the original value. A ratio of the predicted value to the original value is introduced to quantify the comparison. If the ratio is larger than 1, it implies that the value is overpredicted. It should also be noted that for a given breaking wave and a given quantile, the predicted value is deterministic, while the actual value due to the breaking wave is very random, due to the inherent nature of slamming events [21]. As a result, the ratio of the predicted value to the original value is expected to vary in a certain range. However, if the ratio is more likely to be larger than 1 (i.e. predicted value overestimated), it indicates that such prediction is conservative, which is more desirable from the design point of view.

The ratio of the peak force from the predicted force time history to the peak force from the reconstructed force time history is calculated for each individual wave. The values of the ratio for all 176 waves are plotted in Fig. 15 for four different quantiles. The ratio points in the figure range from about 0.5 to about 6, with a concentration between 1 and 3. Depending on the selected quantile,

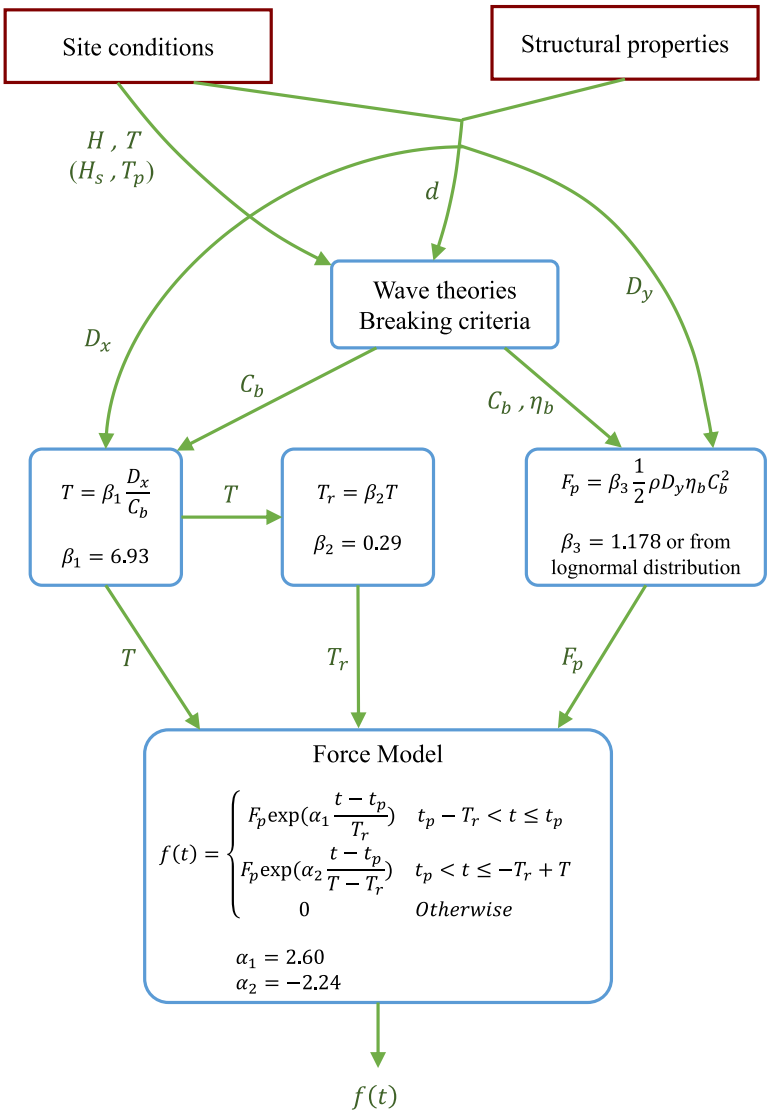

Fig. 13. Application flow chart of the slamming force time series model.

the points scatter around different values. The overestimation rates of peak force for the predicted slamming force with a quantile of 50%, 90%, 95% and 99% are approximately 0.5, 0.90, 0.96 and 0.99, respectively. The overestimation rate is fairly close to the corresponding quantile, this is because the predicted peak force is proportional to ζ_3, which is determined based on the given quantile.

Total impulse (i.e. the integral of the force over time) is another important parameter that characterizes the slamming force. Similar to the peak force, the ratio of the impulse from the predicted force time history to the impulse from the reconstructed force time history is calculated for each individual wave. Fig. 16 depicts the values of the ratio for all 176 waves and for four different quantiles. The points of impulse ratio are distributed in a narrower range in the figure compared to the points of peak force ratio in Fig. 15, indicating that the impulse values tend to be overestimated to a less extend than the peak force values. However, the overestimation rates of impulse for the predicted slamming force with a quantile of 50%, 90%, 95%, and 99% are approximately 0.61, 0.94, 0.97 and 1.0, respectively. Therefore, for a given quantile (e.g. 95%), the impulse of more waves tend to be overestimated compared to the peak force.

It should be noted that in Figs. 15 and 16 wave IDs larger than about 90 correspond to case 6, which has 5 runs with the same preset condition. The other cases have only 1 or 2 runs, i.e., much fewer waves.

Considering the verification results for peak force and impulse above, the developed force model can give a conservative prediction of slamming force time histories, which can be used for engineering design purposes, provided that the ζ_3 value or the quantile is selected carefully to account for the inherent randomness of slamming forces. Such value should be large enough to ensure that the predicted slamming force is conservative enough to provide a safe design. A highly conservative prediction of slamming forces

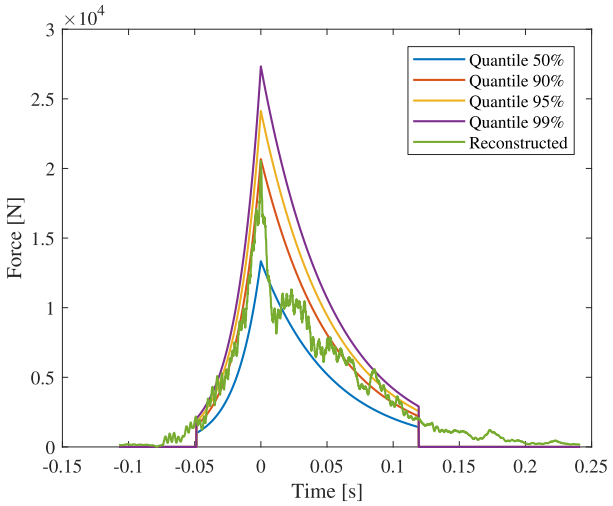

Fig. 14. An exemplary comparison between the original reconstructed slamming force and the predicted slamming forces. Time histories of the predicted slamming forces are estimated according to equation (15) with ζ_3 values corresponding to four quantiles.

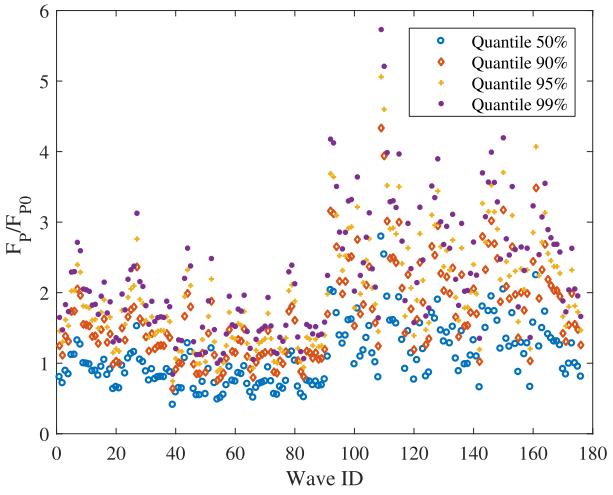

Fig. 15. The ratio of the peak force from the predicted slamming force, F_P, to that of the original reconstructed slamming force, F_{P0}. Four different quantiles are considered when estimating the predicted slamming force.

demands a much stronger structure, which increases its cost. Meanwhile, the value should not be too large, since the probability of waves breaking exactly at the structures is very low. Therefore, the quantile should be chosen based on the balance of structural safety and economy.

6. Discussion

The force model developed in Section 4 is based on the wave cases given in Table 3, in which several different combinations of wave height and wave period were considered. Hence the effect of variable wave conditions is included in the developed force model. The force model consists of five parameters that are independent of waves and structures, i.e. two exponential parameters (α_1, α_2) and three coefficients for calculating wave-dependent parameters (ζ_1, ζ_2 and ζ_3). These five parameters are dimensionless and were estimated at 1:8 scale, which is a relatively large scale compared to commonly used scaling ratios in wave basin model tests [6,22]. The scaling effect on these five parameters is expected to be small. Therefore, the force model can be considered applicable in full scale as well, though it was developed based on model scale data. Air bubbles affect the local pressure distribution significantly, and they might also affect global slamming forces. However, for a jacket structure, this effect is expected to be much less, due to the spatial and temporal averaging that occurs.

Though only one jacket structure was considered for the model development, it is a representative jacket structure for offshore wind applications. The developed force model is applicable to four-leg jackets with waves coming from 0° with respect to the jackets. The application of the model to other jacket types or for waves coming from other directions is not investigated this study. The force

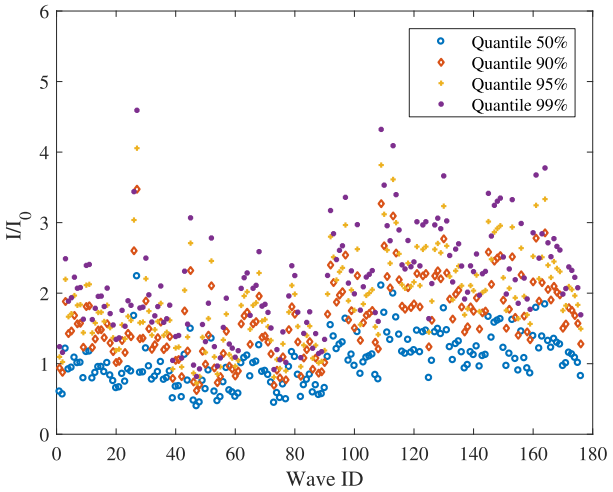

Fig. 16. The ratio of the impulse of the predicted slamming force, I, to that of the original reconstructed slamming force, I_0. Four different quantiles are considered when estimating the predicted slamming force.

model is developed based on shallow water experimental data. The applicability of the model in intermediate water still needs to be studied in the future.

A time-resolved slamming force model as the developed one is essential for the analysis of a jacket structure, because a jacket structure is a multiple degree of freedom (MDOF) system. The slamming can excite modes of the jacket with natural periods that are comparable to the impact duration.

The developed force model has an evident rising time, which is quite different from most of the force models for cylindrical structures given in Table 1. It should be noted that most force models for cylindrical structures were originally developed for 2D slamming forces. When they were extended to 3D slamming problems, the steep fronts of breaking waves were assumed to act on the structures simultaneously, implying that the rising time is neglected. However, in the model tests of the WaveSlam project, it was clearly observed that the wave fronts impacted different parts of the front plane of the structure at different instants in a random manner [23]. Therefore, an exponential increase of the total slamming force before the peak, as observed in this study, can be expected. Actually, even for cylindrical structures, a rising time before the peak was observed in the experiment as well, such as in WiFi JIP project [6].

The fact that the steep fronts of breaking waves do not impact the structure at the same time causes a gradually increasing and then decreasing time history of the resulting slamming forces. Since the force model developed in this study is based on experimental data, such characteristics during the actual slamming events are thus more likely to be accounted for.

In the developed force model, an essential wave parameter is the maximum elevation of the breaking wave η_b. It is used to determine the breaking wave celerity C_b for shallow water, and it affects the values of duration T, rising time T_r, and peak force F_p. In the above model verification section, η_b was determined based on measured data. However, how to properly estimate η_b for a given sea state is very challenging. In addition, the total wave force consists of a quasi-static part and a dynamic part (i.e. slamming forces). The quasi-static load is estimated by the Morison equation, in which the wave kinematics, such as velocity and acceleration of the fluid, are required. These wave kinematics should also be properly estimated.

For a given sea state with a significant wave height H_s and peak period T_p, whether it is likely to include breaking waves should be first justified. During the model tests of the WiFi JIP, it was found that at steep sea states, some waves lead to impulse like impacts due to their steep fronts. The limiting sea state steepness above which such behavior was observed was found to be [6]

$$\frac{H_s}{L_p} > 0.04 \tag{21}$$

in which L_p is the peak wave length. It can be estimated by using the linear dispersion relationship based on known peak period T_p and water depth d. If the sea state is identified to potentially contain breaking waves, two approaches can be applied to determine η_b and the wave kinematics. One approach is to use a fully nonlinear numerical wave tank to generate the time series of wave elevation and wave kinematics. This approach is employed by Peeringa et al. [24] to generate stochastic nonlinear waves using the nonlinear potential flow solver OceanWave3D [25]. The other approach is to embed a stream function wave into a linear irregular wave realization. The extreme wave from an irregular wave time series is substituted with a stream function regular wave. This approach has been employed in engineering practice of offshore wind industry. Recent development of this approach includes a new method proposed by Pierella et al. [26] to embed a stream function wave based on the Hilbert transform.

For sea states containing breaking waves, the time series of the slamming forces on a structure can be determined for a specific percentile of ζ_3. For these sea states, the target return period should account for the occurrence of the sea states, the occurrence of plunging breaking waves, and the percentile of ζ_3. Therefore, the characteristic load with a target return period is not determined by

merely selecting a percentile of ζ_3. Both the occurrence probability of the sea states and the occurrence probability of plunging breaking waves should be properly selected as well.

7. Conclusion

In this study, a force model was developed for estimating global slamming forces due to plunging breaking waves on jacket structures, based on statistical analyses of experimental data from the WaveSlam project. Given a sea state, this force model provides a deterministic and conservative prediction of the slamming force time history, which inherently has random features.

The force model was developed by refining a five-parameter model proposed by Tu et al. [12], using a total of 176 individual breaking waves, under six wave conditions. For each individual breaking wave, the time history of the resulting slamming force was reconstructed based on hammer test data and wave test data, and the wave parameters were acquired from a wave elevation measurement.

The parameters involved in the force model, including two exponential parameters and three wave-dependent parameters (i.e. duration T, rising time T_r and peak force F_p), were determined by using the acquired slamming force time histories and wave parameters. The two exponential parameters were found to be constant, by applying weighted linear regression to the slamming force time histories. The wave-dependent parameters were expressed by three dimensionless parameters (i.e. duration coefficient ζ_1, rising time coefficient ζ_2 and peak force coefficient ζ_3), together with the acquired wave parameters and the structural dimensions. The dimensionless parameters were then determined in a statistical way. It was found that ζ_1 and ζ_2 are approximately constant, and ζ_3 follows a lognormal distribution. The value of ζ_3 is recommended to be determined by choosing a quantile that can give a conservative prediction.

The developed force model was verified against the original reconstructed force time histories. Since the model was developed based on regular wave cases, the applicability of the model to irregular waves should be validated against model test data or field measurements. It is also worthy of studying how to employ the slamming force model in probability-based design of jacket structures.

Acknowledgment

This work has been supported by the European Community's Seventh Framework Programme through the grant to the budget of the Integrating Activity HYDRALAB IV within the Transnational Access Activities, Contract no. 261520.

Additional financial support from NOWITECH FME (Research Council of Norway, contract no. 193823) is gratefully acknowledged.

References

[1] Faltinsen O. Sea loads on ships and offshore structures. Cambridge University Press; 1993.
[2] von Karman T. The impact on seaplane floats during landing Technical Note, NO. 321 National Advisory Committee on Aeronautics; 1929.
[3] Wagner H. Über Stoß-und Gleitvorgänge an der Oberfläche von Flüssigkeiten. ZAMM-J Appl Math Mech/Zeitschrift für Angewandte Mathematik und Mechanik 1932;12(4):193–215.
[4] Wienke J, Oumeraci H. Breaking wave impact force on a vertical and inclined slender pile - theoretical and large-scale model investigation. Coastal Eng 2005;52:435–62. http://dx.doi.org/10.1016/j.coastaleng.2004.12.008.
[5] International Electrotechnical Commission (IEC). IEC 61400–61403, Wind turbines - part 3: design requirements for offshore wind turbines; 1.0. 2009.
[6] Burmester S, de Ridder EJ, Wehmeyer C, Asp E, Gujer P. Comparing different approaches for calculating wave impacts on a monopile turbine foundation. ASME 2017 36th international conference on ocean, offshore and arctic engineering. American Society of Mechanical Engineers; 2017. V010T09A063.
[7] Tu Y, Cheng Z, Muskulus M. A review of slamming load application to offshore wind turbines from an integrated perspective. Energy Procedia 2017;137:346–57.
[8] Goda Y, Haranaka S, Kitahata M. Study of impulsive breaking wave forces on piles. Report of Port and Harbour Technical Research Institute. 5. 1966. p. 1–30. (6).
[9] Campbell I, Weynberg P. Measurement of parameters affecting slamming. University of Southampton, Department of Aeronautics and Astronautics; 1980.
[10] Cointe R, Armand JL. Hydrodynamic impact analysis of a cylinder. J Offshore Mech Arctic Eng 1987;109(3):237–43.
[11] Jose J. Offshore structures exposed to large slamming wave loads. Norway: University of Stavanger; 2017.
[12] Tu Y, Cheng Z, Muskulus M. Global slamming forces on jacket structures for offshore wind applications. Mar Struct 2018;58:53–72.
[13] Tu Y, Grindstad TC, Muskulus M. Inverse estimation of local slamming loads on a jacket structure. J Offshore Mech Arctic Eng 2017;139(6). 061601.
[14] Arntsen Ø, Obhrai C, Gudmestad O. Data storage report: wave slamming forces on truss structures in shallow water Technical Report, WaveSlam (HylV-FZK-05) Norwegian University of Science and Technology; 2013.
[15] Tørum A. Wave slamming forces on truss structures in shallow water Technical Report, Version 2011-10–03 Department of Civil and Transport Engineering, Norwegian University of Science and Technology; 2011
[16] Cleveland WS. Robust locally weighted regression and smoothing scatterplots. J Am Stat Assoc 1979;74(368):829–36. http://dx.doi.org/10.1080/01621459.1979.10481038.
[17] Tu Y, Muskulus M. Statistical properties of local slamming forces on a jacket structure in offshore wind applications. In: Proceedings of 26th international ocean and polar engineering conference. vol.1. Rhodes, Greece: International Society of Offshore and Polar Engineers; 2016. p. 206–13.
[18] Bevington PR, Robinson DK. Data reduction and error analysis for the physical sciences. McGraw-Hill; 2003.
[19] Tanimoto K, Takahashi S, Kaneko T, Shiota K. Impulsive breaking wave forces on an inclined pile exerted by random waves. Coast Eng Proc 1986;1(20):2288–302. http://dx.doi.org/10.1061/9780872626003.168.
[20] Mei CC, Stiassnie M, Yue DK. Theory and applications of ocean surface waves: nonlinear aspects. World Scientific; 2005.
[21] Lian G, Haver SK. Estimating long-term extreme slamming from breaking waves. J Offshore Mech Arctic Eng 2016;138(5):051101.
[22] Loukogeorgaki E, Lentsiou EN, Chatjigeorgiou IK, et al. Experimental investigation of slamming loading on a three-legged jacket support structure of offshore wind turbines. Proceedings of 26th international ocean and polar engineering conference. vol.1. Rhodes, Greece: International Society of Offshore and Polar Engineers; 2016. p. 192–8.
[23] Tu Y, Muskulus M, Arntsen ØA. Experimental analysis of slamming load characteristics for truss structures in offshore wind applications. J Ocean Wind Energy 2015;2(3):138–45.
[24] Peeringa JM, Hermans KW. Impact of new slamming wave design method on the structural dynamics of a classic, modern and future offshore wind turbine. ASME 2017 36th international conference on ocean, offshore and arctic engineering. American Society of Mechanical Engineers; 2017. p. V010T09A071.
[25] Engsig-Karup AP, Bingham HB, Lindberg O. An efficient flexible-order model for 3D nonlinear water waves. J Comput Phys 2009;228(6):2100–18.
[26] Pierella F, Stenbro R, Oggiano L, de Vaal J, Nygaard TA, Krokstad J, et al. Stream function wave embedment into linear irregular seas: a new method based on the hilbert transform. The 27th international ocean and polar engineering conference. International Society of Offshore and Polar Engineers; 2017.